Progress In Electromagnetics Research, PIER 77, 309–328, 2007

TIME DOMAIN ANALYSIS OF ACTIVE TRANSMISSION LINE USING FDTD TECHNIQUE (APPLICATION TO MICROWAVE/MM-WAVE TRANSISTORS)

K. Afrooz, A. Abdipour, A. Tavakoli, and M. Movahhedi

Microwave/mm-Wave & Wireless Communication Research Lab
Radio Communication Center of Excellence
Electrical Engineering Department
Amirkabir University of Technology
424 Hafez Ave., Tehran, Iran

Abstract—In this paper, an accurate modeling procedure for GaAs MESFET as active coupled transmission line is presented. This model can consider the effect of wave propagation along the device electrodes. In this modeling technique the active multiconductor transmission line (AMTL) equations are obtained, which satisfy the TEM wave propagation along the GaAs MESFET electrodes. This modeling procedure is applied to a GaAs MESFETs by solving the AMTL equations using Finite-Difference Time-Domain (FDTD) technique. The scattering parameters are computed from time domain results over a frequency range of 20–220 GHz. This model investigates the effect of wave propagation along the transistor more accurate than the slice model, especially at high frequencies.

1. INTRODUCTION

Due to the required increasing performance and lower cost, monolithic microwave integrated circuits (MMICs) are evolving with a large number of closely packed passive and active structures, several levels of transmission lines and discontinuities on the same chip [1]. With the increasing flow of data in telecommunication world, the high-performance electronics that are based on MMIC technologies operating at high speeds, frequencies, and sometime over very broad bandwidths are needed. Also by increasing the operating frequency, devices and circuits need to more and more accurate techniques for modeling and simulation [2]. For accurate device modeling an

electromagnetic interaction must be taken into account, especially when the gate width is on the order of the wavelength [2]. When the device dimension become comparable to the wavelength the input active transmission line, the gate electrode, has a different reactance from the output transmission line, the drain electrode. Therefore, they exhibit different phase velocities for the input and output signals. So by increasing the frequency or device dimension the phase cancellation due to the phase velocity mismatching will effect the performance of the device [3, 4]. In such cases, wave propagation effect influences the electrical performance of the device, so this phenomena needs to be considered accurately in device modeling. The full wave analysis and global modeling approach can be used to consider the wave propagation effect along the device structure, accurately. But, this type of analysis is time consuming and needs a huge CPU time. Although, some efficient numerical methods have been recently proposed for simulation time reduction [5–9], but it sounds that this analysis approach needs more attention for implementing in simulation software. On the other hand, device behavior in high frequencies can be well described using semi-distributed model which can be easily implemented in CAD routines of simulators [9–12]. But the semi-distributed model cannot consider wave propagation effect and phase cancellation on the electrical performance of the device [2]. In the paper, we propose a new modeling procedure for GaAs MESFET which can consider the effect of wave propagation along the device electrodes. In the proposed approach, the transverse electromagnetic (TEM) wave propagation is investigated on the electrodes of the device. In this model, the device width is divided into infinity segments. Each segment is considered as a combination of three coupled lines and a conventional equivalent circuit of a GaAs MESFET. Its parameters in the MESFET model circuit are obtained from DC and low frequency measurements (Fig. 2). The transmission line theory is applied to a segment of transistor to obtain the wave equation in a GaAs MESFET structure. Now this system of differential equations (active multiconductor transmission line (AMTL) equation) must be solved. Since a time domain analytical solution doesn't exist for this system, this problem is needed to solve using a numerical technique. The Finite Difference Time Domain (FDTD) method is widely used in solving various kinds of electromagnetic problems, wherein lossy, nonlinear, inhomogeneous media and transient problem can be considered [13]. This technique is used to solve the obtained equations. By applying this modeling technique, the scattering parameters of a sub micrometer-gate GaAs transistor are calculated over a frequency range of 20–220 GHz. The results achieved from this model (Fully distributed) are compared with

slice model. It is shown, at the low frequencies, the results of semi-distributed and fully distributed models are the same. By increasing the frequency, the results of two models are not in a good agreement. Because the fully distributed model is a modified version of the semi-distributed one when the number of slices increases to the infinity and consider the wave propagation, we expect the proposed method become more accurate. This is confirmed by comparing the S-parameters calculated using both models over a wide frequency band.

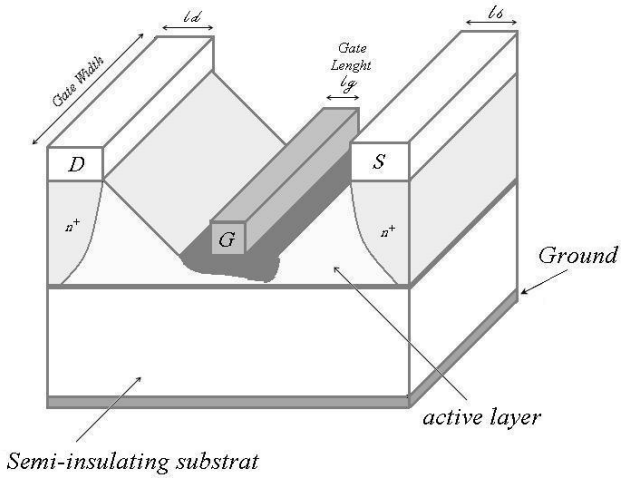

Figure 1. The schematic of GaAs MESFET.

2. MODEL IDENTIFICATION

A typical millimeter-wave field effect transistor is shown in Fig. 1. The device consists of three coupled electrodes fabricated on a thin layer of GaAs supported by a semi-insulating GaAs substrate. As operating frequency of the microwave GaAs MESFETs increase to the millimeter wave range, the dimensions of the electrodes become comparable to the wavelength. In this situation the transmission line properties of the electrodes need to be considered [22–24]. Fully distributed model is one of the accurate models which is applied to calculate the effect of wave propagation along the electrodes of a GaAs MESFET.

For low enough frequencies, the longitudinal EM field is very small in magnitude as compared to the transverse field [2, 3]. Therefore we can consider quasi-TEM modes and the generalized active multiconductor transmission line (AMTL)' equation. This equation can be used to describe the instantaneous voltage and current

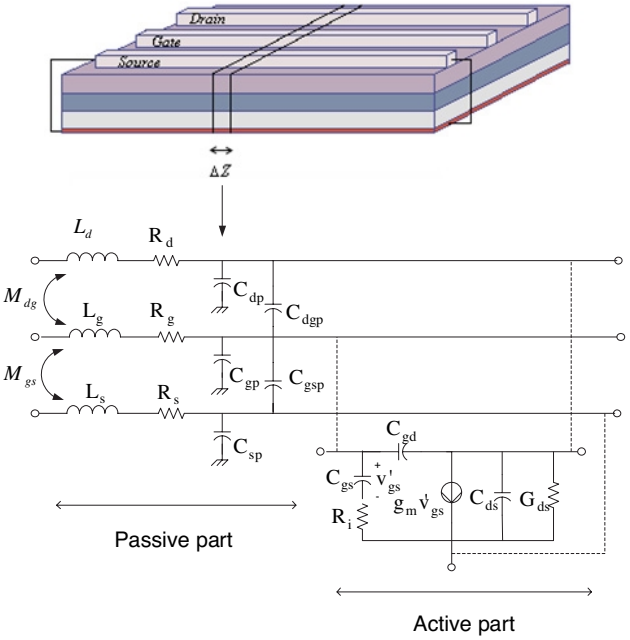

Figure 2. An equivalent circuit model of a differential length of a transistor (AMTL).

relationship in the transistor. Consider an element portion of length of a three-Active transmission line. We intend to find an equivalent circuit for this line and derive the transistor equations. An equivalent circuit of a portion of the transistor is shown in Fig. 2. Each segment is represented by a 6-ports equivalent circuit which combines a conventional MESFET small signal circuit model and another circuit element to account the coupled transmission line effect of the electrode structure where the all parameters are per unit length. By applying kirchhoff's current law to the left loop of the circuit in Fig. 2 and in the limit as $\Delta z \to 0$, we obtain the following three equations:

$$\frac{\partial}{\partial z}I_d(z,t) + C_1\frac{\partial}{\partial t}V_d(z,t) - C_{12}\frac{\partial}{\partial t}V_g(z,t) - C_{13}\frac{\partial}{\partial t}V_s(z,t) + G_{ds}(V_d(z,t) - V_s(z,t)) + G_m\acute{V}_g(z,t) = 0 \quad (1)$$

$$\frac{\partial}{\partial z}I_g(z,t) - C_{12}\frac{\partial}{\partial t}V_d(z,t) + C_2\frac{\partial}{\partial t}V_g(z,t) - C_{23}\frac{\partial}{\partial t}V_s(z,t) + C_{gs}\frac{\partial}{\partial t}\acute{V}_g(z,t) = 0 \quad (2)$$

$$\frac{\partial}{\partial z}I_s(z,t)-C_{13}\frac{\partial}{\partial t}V_d(z,t)-C_{23}\frac{\partial}{\partial t}V_g(z,t)+C_3\frac{\partial}{\partial t}V_s(z,t)-C_{gs}\frac{\partial}{\partial t}\acute{V}_g(z,t)$$
$$-G_{ds}(V_d(z,t)-V_s(z,t))-G_m\acute{V}_g(z,t)=0 \tag{3}$$

Also, we can write an extra equation:

$$V_g(\acute{z},t)+V_s(z,t)+R_iC_{gs}\frac{\partial}{\partial t}\acute{V}_g(z,t)-V_g(z,t)=0 \tag{4}$$

where
$C_1=C_{dp}+C_{ds}+C_{dsp}+C_{dg}+C_{dgp}$
$C_2=C_{gp}+C_{gsp}+C_{dg}+C_{dgp}$
$C_3=C_{sp}+C_{ds}+C_{dsp}+C_{gsp}$
$C_{12}=C_{dg}+C_{dgp}$
$C_{13}=C_{ds}+C_{dsp}$
$C_{23}=C_{gsp}$
similarly, applying the kirchhoff's voltage law to the main node of the circuit and in the limit as $\Delta z\to 0$ in Fig. 2 gives:

$$\frac{\partial}{\partial z}V_d(z,t)+R_dI_d(z,t)+L_d\frac{\partial}{\partial t}V_d(z,t)+M_{dg}\frac{\partial}{\partial t}V_g(z,t)$$
$$+M_{ds}\frac{\partial}{\partial t}V_s(z,t)=0 \tag{5}$$
$$\frac{\partial}{\partial z}V_g(z,t)+R_gI_g(z,t)+L_g\frac{\partial}{\partial t}V_g(z,t)+M_{dg}\frac{\partial}{\partial t}V_d(z,t)$$
$$+M_{gs}\frac{\partial}{\partial t}V_s(z,t)=0 \tag{6}$$
$$\frac{\partial}{\partial z}V_s(z,t)+R_sI_s(z,t)+L_s\frac{\partial}{\partial t}V_s(z,t)+M_{ds}\frac{\partial}{\partial t}V_d(z,t)$$
$$+M_{gs}\frac{\partial}{\partial t}V_g(z,t)=0 \tag{7}$$

The above equations could be simplify in two matrix equations as follows:

$$\frac{\partial}{\partial z}\begin{pmatrix}I_d\\I_g\\I_s\\0\end{pmatrix}+\frac{\partial}{\partial t}\begin{pmatrix}C_1&-C_{12}&-C_{13}&0\\-C_{12}&C_2&-C_{23}&C_{gs}\\-C_{13}&-C_{23}&C_3&-C_{gs}\\0&0&0&R_iC_{gs}\end{pmatrix}\begin{pmatrix}V_d\\V_g\\V_s\\\acute{V}_g\end{pmatrix}$$
$$+\begin{pmatrix}G_{ds}&0&-G_{ds}&G_m\\0&0&0&0\\-G_{ds}&0&G_{ds}&-G_m\\0&-1&1&1\end{pmatrix}\begin{pmatrix}V_d\\V_g\\V_s\\\acute{V}_g\end{pmatrix}=0 \tag{8}$$

$$\frac{\partial}{\partial z}\begin{pmatrix} V_d \\ V_g \\ V_s \end{pmatrix} + \frac{\partial}{\partial t}\begin{pmatrix} L_d & M_{dg} & M_{ds} \\ M_{dg} & L_g & M_{gs} \\ M_{ds} & M_{gs} & L_s \end{pmatrix}\begin{pmatrix} I_d \\ I_g \\ I_s \end{pmatrix} + \begin{pmatrix} R_d & 0 & 0 \\ 0 & R_g & 0 \\ 0 & 0 & R_s \end{pmatrix}\begin{pmatrix} I_d \\ I_g \\ I_s \end{pmatrix} = 0 \tag{9}$$

where I_d, V_d, I_g, V_g and I_s, V_s are the drain, gate and source currents and voltages, respectively and $\acute{V}_g$ is gate-source capacitance voltage.

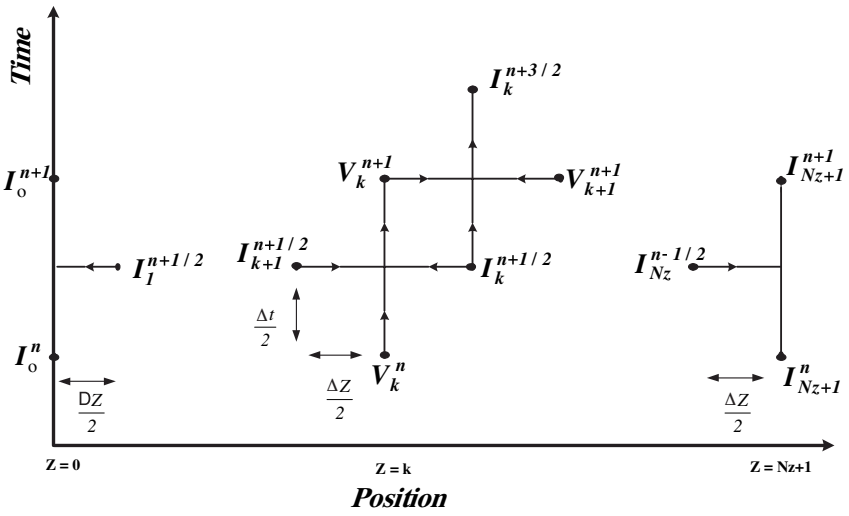

Figure 3. The relation between the spatial and temporal discretization to achieve second-order accuracy in the discretization of the derivatives.

3. THE FDTD SOLUTION OF THE AMTL EQUATION

The fully distributed model of a GaAs MESFET is embodied in the AMTL equations

$$\frac{\partial}{\partial z}\acute{\mathbf{I}}(z,t) + \mathbf{C}\frac{\partial}{\partial t}\acute{\mathbf{V}}(z,t) + \mathbf{G}\acute{\mathbf{V}}(z,t) = 0 \tag{10}$$

$$\frac{\partial}{\partial z}\mathbf{V}(z,t) + \mathbf{L}\frac{\partial}{\partial t}\mathbf{I}(z,t) + \mathbf{R}\mathbf{I}(z,t) = 0 \tag{11}$$

where

$$\mathbf{V}(z,t) = [V_d(z,t), V_g(z,t), V_s(z,t)]^T \quad (12)$$

$$\mathbf{I}(z,t) = [I_d(z,t), I_g(z,t), I_s(z,t)]^T \quad (13)$$

$$\mathbf{V}(\acute{z},t) = [V_d(z,t), V_g(z,t), V_s(z,t), \acute{V}_g(z,t)]^T \quad (14)$$

$$\acute{\mathbf{I}}(z,t) = [I_d(z,t), I_g(z,t), I_s(z,t), 0]^T \quad (15)$$

Now a suitable technique should be selected to solve the AMTL equations. One of the best methods which can be used to find the solution of AMTL equation is FDTD technique. The FDTD technique seeks to approximate the derivatives with regard to discrete solution points defined by the spatial and temporal cells [13–15]. The AMTL equations are coupled, first-order partial differentional equations like Maxwell's equations. Applications of the FDTD method to the full-wave solution of Maxwell's equations have shown that accuracy and stability of the solution is achieved if we choose the electric and magnetic field solution points to alternate in space and be separated by one-half the position discretization, e.g., $\Delta z/2$ [14]. We choose the solution times for these two equations to also be interlaced in time and separated by $\Delta t/2$. In order to insure stability of the discretization and to insure second-order accuracy we interlace the N_z+1 voltage points, $V_1, V_2, \ldots, V_{N_z}, V_{N_z+1}$, and the N_z current points, $I_1, I_2, \ldots, I_{N_z}$, as shown in Fig. 3 [16–19]. Each voltage and adjacent current solution point is separated by $\Delta z/2$. In addition, the time points are also interlaced, and each voltage time point and adjacent current time point are separated by $\Delta t/2$ as illustrated in Fig. 3. With applying the finite difference approximation to (10) and (11) gives:

$$\frac{V_{k+1}^{n+1} - V_k^{n+1}}{\Delta z} + \mathbf{L}\frac{I_k^{n+\frac{3}{2}} - I_k^{n+\frac{1}{2}}}{\Delta t} + \mathbf{R}\frac{I_k^{n+\frac{3}{2}} + I_k^{n+\frac{1}{2}}}{2} = 0 \quad (16)$$

$$\frac{\acute{I}_k^{\,n+\frac{1}{2}} - \acute{I}_{k-1}^{\,n+\frac{1}{2}}}{\Delta z} + \mathbf{C}\frac{\acute{V}_k^{n+1} - \acute{V}_k^n}{\Delta t} + \mathbf{G}\frac{\acute{V}_k^{n+1} + \acute{V}_k^n}{2} = 0 \quad (17)$$

where we denote

$$\mathbf{V}_i^j \equiv V((i-1)\Delta z, j\Delta t) \quad (18)$$

$$\acute{\mathbf{V}}_i^j \equiv \acute{\mathbf{V}}((i-1)\Delta z, j\Delta t) \quad (19)$$

$$\mathbf{I}_i^j \equiv \mathbf{I}((i-\frac{1}{2})\Delta z, j\Delta t) \quad (20)$$

$$\acute{\mathbf{I}}_i^j \equiv \acute{\mathbf{I}}((i-\frac{1}{2})\Delta z, j\Delta t) \quad (21)$$

Solving these equations give the required recursion relations:

$$\acute{\mathbf{V}}_k^{n+1} = \left(\frac{\mathbf{C}}{\Delta t} + \frac{\mathbf{G}}{2}\right)^{-1} \left\{ \left(\frac{\mathbf{C}}{\Delta t} - \frac{\mathbf{G}}{2}\right) \acute{\mathbf{V}}_k^n - \frac{\acute{\mathbf{I}}_k^{n+\frac{1}{2}} - \acute{\mathbf{I}}_{k-1}^{n+\frac{1}{2}}}{\Delta z} \right\} \quad (22)$$

$$\mathbf{I}_k^{n+\frac{3}{2}} = \left(\frac{\mathbf{L}}{\Delta t} + \frac{\mathbf{R}}{2}\right)^{-1} \left\{ \left(\frac{\mathbf{L}}{\Delta t} - \frac{\mathbf{R}}{2}\right) \mathbf{I}_k^{n+\frac{1}{2}} - \frac{\mathbf{V}_{k+1}^{n+1} - \mathbf{V}_k^{n+1}}{\Delta z} \right\} \quad (23)$$

The leap-frog method is used to solving the AMTL equations because of its simplicity and accuracy. First, the solutions start with an initially relaxed line having zero voltage and current values. Then, voltages along the electrode of transistor are solved for a fixed time from (22) in terms of the previous solutions and then currents are solved for from (23) in terms of these and previous values.

3.1. Boundary Condition

The Equation (22) for $k = 0$ and $k = N_z + 1$ become

$$\acute{\mathbf{V}}_1^{n+1} = \left(\frac{\mathbf{C}}{\Delta t} + \frac{\mathbf{G}}{2}\right)^{-1} \left\{ \left(\frac{\mathbf{C}}{\Delta t} - \frac{\mathbf{G}}{2}\right) \acute{\mathbf{V}}_1^n - \frac{\acute{\mathbf{I}}_1^{n+\frac{1}{2}} - \acute{\mathbf{I}}_0^{n+\frac{1}{2}}}{\frac{\Delta z}{2}} \right\} \quad (24)$$

$$\acute{\mathbf{V}}_{Nz+1}^{n+1} = \left(\frac{\mathbf{C}}{\Delta t} + \frac{\mathbf{G}}{2}\right)^{-1} \left\{ \left(\frac{\mathbf{C}}{\Delta t} - \frac{\mathbf{G}}{2}\right) \acute{\mathbf{V}}_{Nz+1}^n - \frac{\acute{\mathbf{I}}_{Nz+1}^{n+\frac{1}{2}} - \acute{\mathbf{I}}_{Nz}^{n+\frac{1}{2}}}{\frac{\Delta z}{2}} \right\} \quad (25)$$

By considering Fig. 3 this equation requires that we replace Δz with $\frac{\Delta z}{2}$ only for $k = 1$ and $k = N_z + 1$. Referring Fig. 4 we will denote the currents at the source point ($z = 0$) as I_0 and at the load point ($z = L$) as $I_{N_{z+1}}$. By substituting this notation in to (24) we obtain:

$$\mathbf{I}_\circ = \frac{\mathbf{V}_{in}^n + \mathbf{V}_{in}^{n+1} - \mathbf{V}_1^n - \mathbf{V}_1^{n+1}}{2\mathbf{R}_s} \quad (26)$$

where

$$\mathbf{V}_{in} = \begin{pmatrix} V_{ind} \\ V_{ing} \\ V_{ins} \end{pmatrix}, \quad \mathbf{G}_s = \frac{1}{\mathbf{R}_s} = \begin{pmatrix} G_{sd} & 0 & 0 \\ 0 & G_{sg} & 0 \\ 0 & 0 & G_{ss} \end{pmatrix}$$

$$\acute{\mathbf{I}}_\circ = \frac{\acute{\mathbf{V}}_{in}^n + \acute{\mathbf{V}}_{in}^{n+1} - \acute{\mathbf{V}}_1^n - \acute{\mathbf{V}}_1^{n+1}}{2\acute{\mathbf{R}}_s} \quad (27)$$

where

$$\acute{\mathbf{V}}_{in} = \begin{pmatrix} V_{ind} \\ V_{ing} \\ V_{ins} \\ 0 \end{pmatrix}, \quad \acute{\mathbf{G}}_s = \frac{1}{\acute{\mathbf{R}}_s} = \begin{pmatrix} G_{sd} & 0 & 0 & 0 \\ 0 & G_{sg} & 0 & 0 \\ 0 & 0 & G_{ss} & 0 \\ 0 & 0 & 0 & 0 \end{pmatrix}$$

Similarly, we impose the terminal constraint at $z = L$ with substituting $I_{N_{z+1}}$ into (25) as follow:

$$\mathbf{I}_{Nz+1} = \frac{\mathbf{V}^n_{Nz+1} + \mathbf{V}^{n+1}_{Nz+1}}{2\mathbf{R}_L} \tag{28}$$

where

$$\mathbf{G}_L = \frac{1}{\mathbf{R}_L} = \begin{pmatrix} G_{Ld} & 0 & 0 \\ 0 & G_{Lg} & 0 \\ 0 & 0 & G_{Ls} \end{pmatrix}$$

$$\acute{\mathbf{I}}_{Nz+1} = \frac{\acute{\mathbf{V}}^n_{Nz+1} + \acute{\mathbf{V}}^{n+1}_{Nz+1}}{2\acute{\mathbf{R}}_L} \tag{29}$$

where

$$\acute{\mathbf{G}}_L = \frac{1}{\acute{\mathbf{R}}_L} = \begin{pmatrix} G_{Ld} & 0 & 0 & 0 \\ 0 & G_{Lg} & 0 & 0 \\ 0 & 0 & G_{Ls} & 0 \\ 0 & 0 & 0 & 0 \end{pmatrix}$$

The finite difference approximation of Equation (17) can be written as follows:
for $k = 1$

$$\begin{aligned} \acute{\mathbf{V}}^{n+1}_1 &= \left(\frac{\mathbf{C}}{\Delta t} + \frac{\mathbf{G}}{2}\right)^{-1} \left\{ \left(\frac{\mathbf{C}}{\Delta t} - \frac{\mathbf{G}}{2}\right) \acute{\mathbf{V}}^n_1 - \frac{\acute{\mathbf{I}}^{n+\frac{1}{2}}_1 - \acute{\mathbf{I}}^{n+\frac{1}{2}}_0}{\frac{\Delta z}{2}} \right\} \\ &= \left(\frac{\mathbf{C}}{\Delta t} + \frac{\mathbf{G}}{2} + \frac{1}{\acute{\mathbf{R}}_s \Delta z}\right)^{-1} \left\{ \left(\frac{\mathbf{C}}{\Delta t} - \frac{\mathbf{G}}{2} - \frac{1}{\acute{\mathbf{R}}_s \Delta z}\right) \acute{\mathbf{V}}^n_1 \right. \\ &\quad \left. - \frac{2}{\Delta z} \left(\acute{\mathbf{I}}^{n+\frac{1}{2}}_1 - \frac{\acute{\mathbf{V}}^n_{in} + \acute{\mathbf{V}}^{n+1}_{in}}{2\acute{\mathbf{R}}_s} \right) \right\} \end{aligned} \tag{30}$$

for $k = 2, 3, \ldots, N_z$

$$\acute{\mathbf{V}}^{n+1}_k = \left(\frac{\mathbf{C}}{\Delta t} + \frac{\mathbf{G}}{2}\right)^{-1} \left\{ \left(\frac{\mathbf{C}}{\Delta t} - \frac{\mathbf{G}}{2}\right) \acute{\mathbf{V}}^n_k - \frac{\acute{\mathbf{I}}^{n+\frac{1}{2}}_k - \acute{\mathbf{I}}^{n+\frac{1}{2}}_{k-1}}{\Delta z} \right\} \tag{31}$$

for $k = N_z + 1$

$$\acute{\mathbf{V}}_{Nz+1}^{n+1} = \left(\frac{\mathbf{C}}{\Delta t} + \frac{\mathbf{G}}{2}\right)^{-1} \left\{ \left(\frac{\mathbf{C}}{\Delta t} - \frac{\mathbf{G}}{2}\right) \acute{\mathbf{V}}_{Nz+1}^{n} - \frac{\acute{\mathbf{I}}_{Nz+1}^{n+\frac{1}{2}} - \acute{\mathbf{I}}_{Nz}^{n+\frac{1}{2}}}{\frac{\Delta z}{2}} \right\} =$$

$$\left(\frac{\mathbf{C}}{\Delta t} + \frac{\mathbf{G}}{2} + \frac{1}{\acute{\mathbf{R}}_L \Delta z}\right)^{-1} \left\{ \left(\frac{\mathbf{C}}{\Delta t} - \frac{\mathbf{G}}{2} - \frac{1}{\acute{\mathbf{R}}_L \Delta z}\right) \acute{\mathbf{V}}_{Nz+1}^{n} + \frac{2}{\Delta z} \acute{\mathbf{I}}_{Nz} \right\} \quad (32)$$

and for Equation (16):
for $k = 2, 3, \ldots, N_z$

$$\mathbf{I}_k^{n+\frac{3}{2}} = \left(\frac{\mathbf{L}}{\Delta t} + \frac{\mathbf{R}}{2}\right)^{-1} \left\{ \left(\frac{\mathbf{L}}{\Delta t} - \frac{\mathbf{R}}{2}\right) \mathbf{I}_k^{n+\frac{1}{2}} - \frac{\mathbf{V}_{k+1}^{n+1} - \mathbf{V}_k^{n+1}}{\Delta z} \right\} \quad (33)$$

The voltages and currents are solved by iterating k for a fixed time and then iterating time.

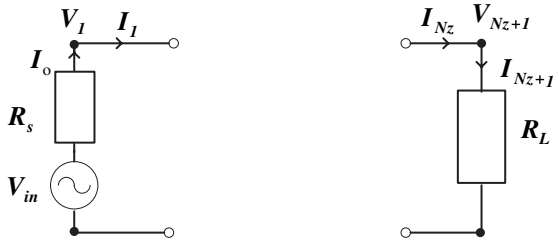

Figure 4. Discretization of the terminal voltages and currents.

4. NUMERICAL RESULTS

The proposed approach is used for modeling a sub micrometer-gate GaAs transistor. The device had a $0.3 \times 560\,\mu$m gate. The input and output nodes were connected to the beginning of the gate electrode and the end of drain electrode. The transistor was biased at $V_{ds} = 3\,$v and $I_{ds} = 10\,$mA. The source and load resistance are $50\,\Omega$. Moreover, the beginning and the end of source electrodes are grounded. A schematic of the considered transistor is shown in Fig. 5. The element values used in the distributed model are given in Tables 1 and 2 [10]. The scattering parameters of this transistor are calculated over a frequency range of 20–220 GHz using fully distributed and slice models from the time domain analysis and are drawn in Fig. 6. It is clearly shown that both results of the fully distributed and the slice models are the

Table 1. Numerical values of distributed model elements for passive part.

The distributed model elements	Numerical values (per unit length)
L_d	780 nH/m
L_s	780 nH/m
L_g	161 nH/m
M_{gd}	360 nH/m
M_{gs}	360 nH/m
M_{ds}	240 nH/m
C_{gp}	0.6 pF/m
C_{dp}	87 pF/m
C_{sp}	148 pF/m
C_{gdp}	29 pF/m
C_{gsp}	29 pF/m
C_{dsp}	61 pF/m
R_d	900 Ω/m
R_s	900 Ω/m
R_g	34300 Ω/m

Table 2. Numerical values of distributed model elements for active part at $V_{ds} = 3$ v and $I_{ds} = 10$ mA.

The distributed model elements	Numerical values (per unit length)
C_{gs}	0.771 nF/m
C_{ds}	0.0178 nF/m
C_{gd}	0.1178 nF/m
G_m	146.42 S/m
R_i	0.002 Ω/m
G_{ds}	15.46 mho/m

same at the low frequency (in this problem under 40 GHz) but by increasing the frequency, the results of two models would be different. In order to test actual predictive capabilities of the propose approach, the model was adopted to predict the electrical behavior of two device structures (a $0.3 \times 840\,\mu$m and a $0.3 \times 1120\,\mu$m). The parameters of

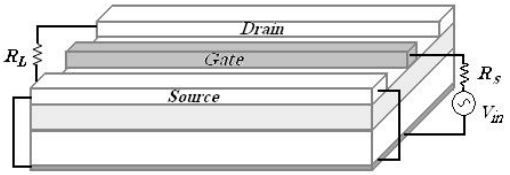

Figure 5. Schematic of the simulated transistor.

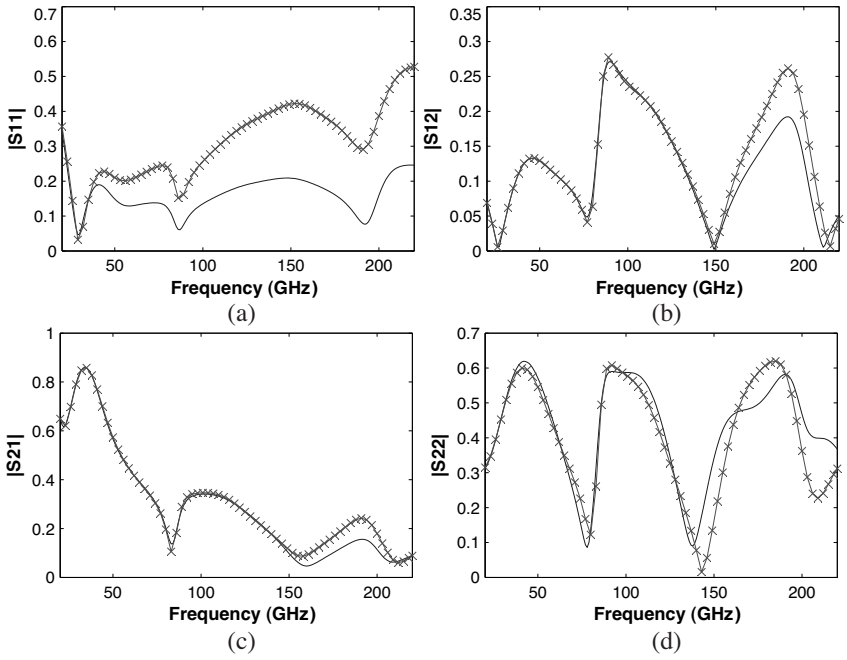

Figure 6. The scattering parameters of transistor with 560 μm gate width. "—" fully distributed model, " $\times$ $\times$ $\times$ " slice model. (a) magnitude of S_{11}, (b) magnitude of S_{21}, (c) magnitude of S_{21}, (d) magnitude of S_{22}.

these transistors is obtained using scaling method [21]. In Figs. 7 and 8 the scattering parameters obtained for two device structures using the new approach and slice model are shown, respectively. It is obvious that by increasing the device dimension and the frequency, difference between fully distributed and slice model also increases. The most obvious difference between two models are appeared for the magnitude of S_{11}.

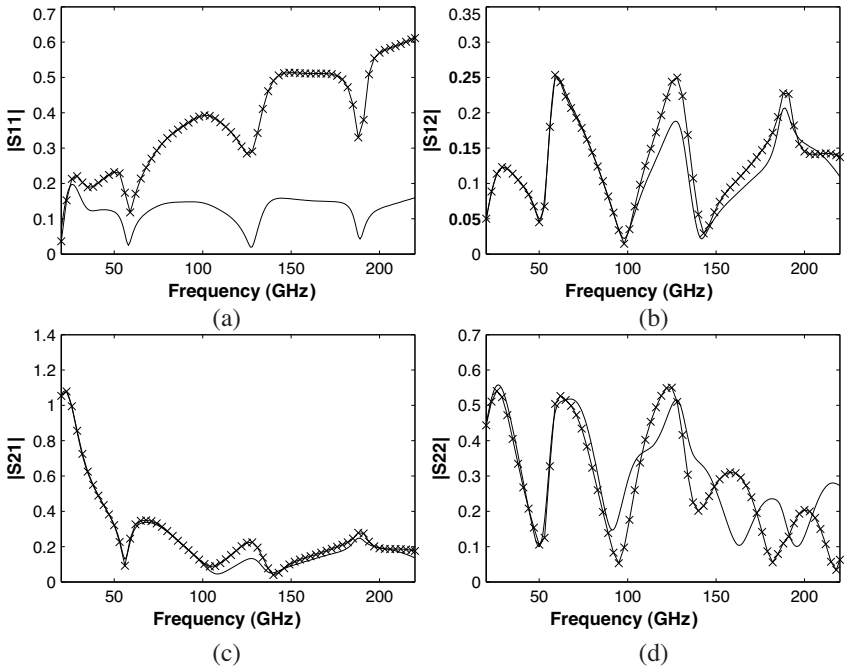

Figure 7. The scattering parameters of transistor with 840 μm gate width. "—" fully distributed model, " $\times$ $\times$ $\times$ " slice model. (a) magnitude of S_{11}, (b) magnitude of S_{21}, (c) magnitude of S_{21}, (d) magnitude of S_{22}.

As the equations show, the fully distributed model is a modify version of slice model when the number of slices has been increased to infinity. Therefore, the results of fully distributed model is more accurate than the slice model, specially at the high frequency applications and devices which their dimensions are comparable with wavelength. It is due to this fact that fully distributed model is based on solving the wave equation in the transistor structure while the slice model is based on circuit modeling. Therefore, the fully distributed model can consider the effect of wave propagation along the device electrode more accurate than the slice model, especially when the device dimension is comparable with the wavelength. Because the gate electrode has a different reactance from the drain electrode, Therefore they exhibit different phase velocities for the input and output signals. By increasing the frequency or device dimension, the phase cancellation phenomena due to the phase velocity mismatching cannot be neglected. This effect can be consider in fully distributed

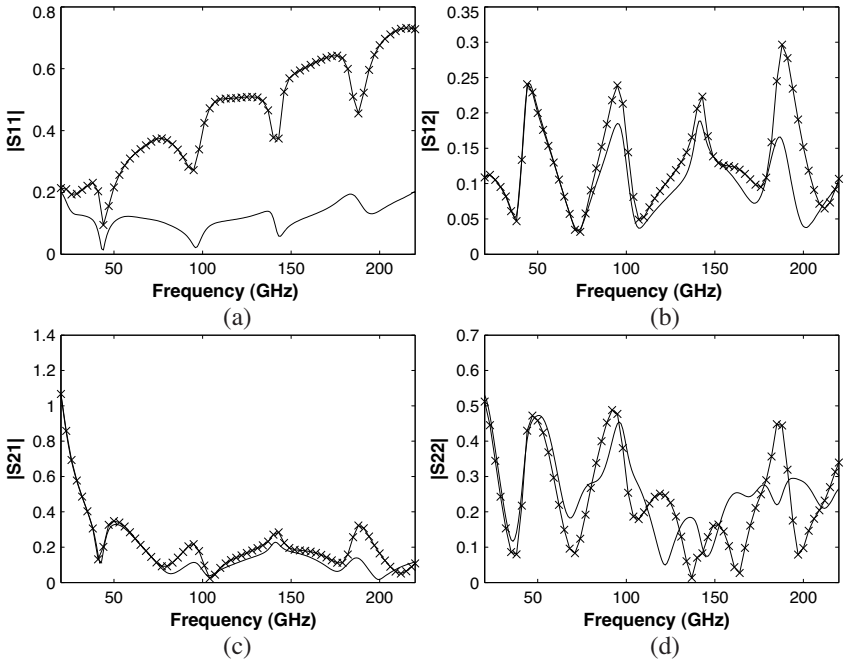

Figure 8. The scattering parameters of transistor with 1120 μm gate width. "—" fully distributed model, " $\times \times \times$ " slice model. (a) magnitude of S_{11}, (b) magnitude of S_{21}, (c) magnitude of S_{21}, (d) magnitude of S_{22}.

model. Fig. 9 depicts the voltage gain as a function of the gate width at 80 GHz. It is obvious that by increasing the gate width, voltage gain decrease periodically due to the phase cancellation. The time domain load voltage obtained from the fully distributed and slice models for a transistor with 560 μm when excited by sinusoidal source (80 GHz) are shown in Fig. 10. The magnitude and the phase of the solution for the fully distributed model is different from slice model. The most important reason for this difference is the phase cancellation that is taken account in to by the fully distributed model. Figs. 11 and 12 show the time domain variation of voltage in the beginning and the end of drain and gate electrodes at 100 GHz frequency using fully distributed model, respectively. Fig. 12 depicts the gate voltage at the beginning and the end of electrode. The magnitude of voltage at the end of the gate electrode is less than the voltage at the beginning the gate electrode. This is mainly due to the gate ohmic resistance. Fig. 11 shows the transistor has amplification at the end of the drain

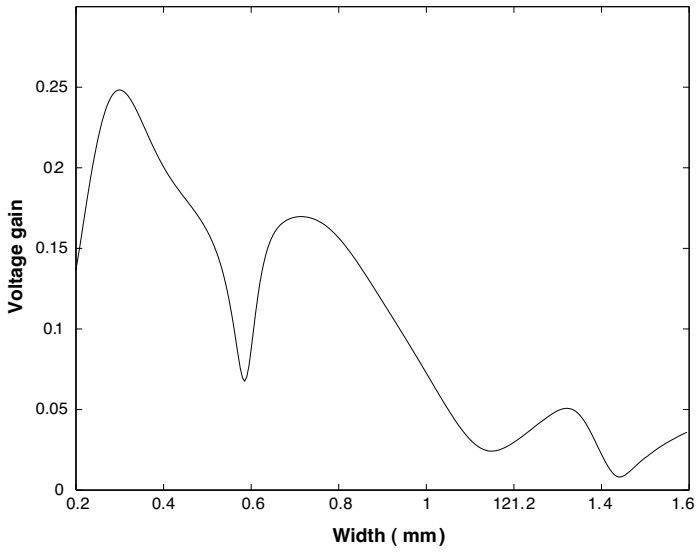

Figure 9. The transistor voltage gain versus gate width at 80 GHz frequency.

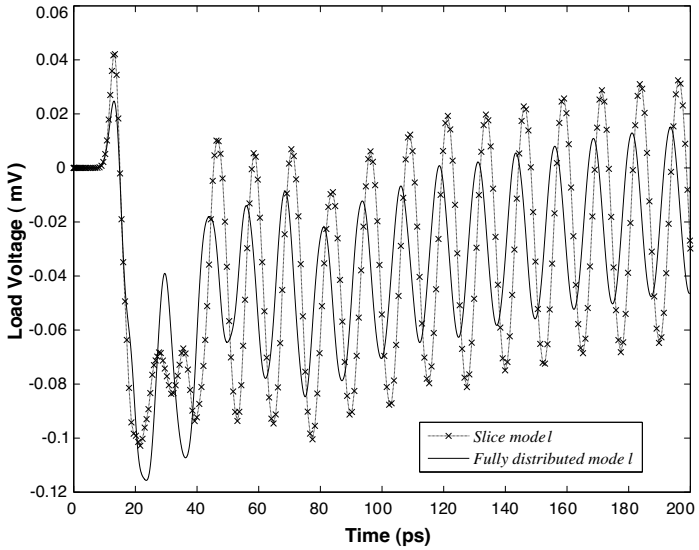

Figure 10. Time domain load voltage from slice and fully distributed models at 100 GHz frequency.

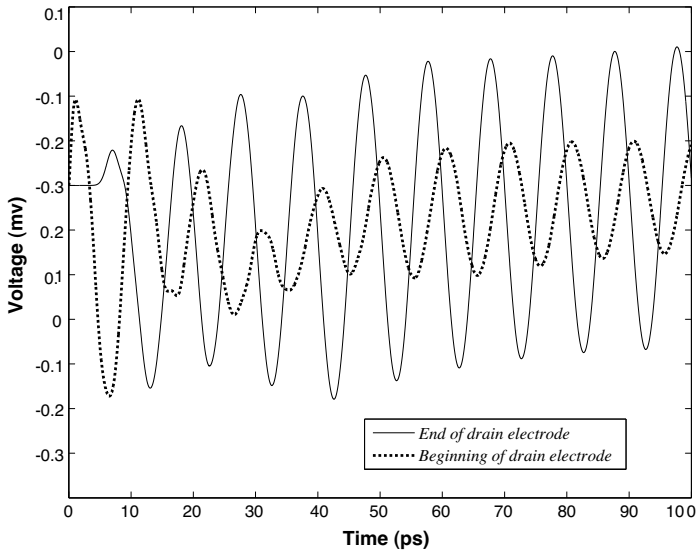

Figure 11. The voltage of transistor with 560 μm gate width at the beginning and end of the drain electrode.

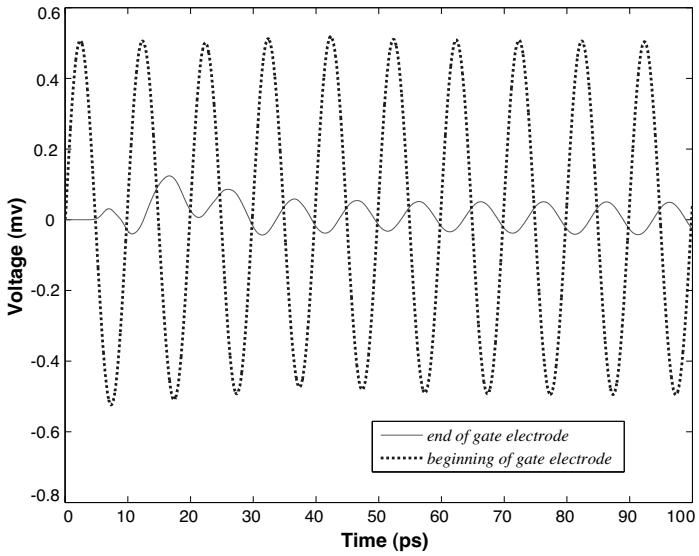

Figure 12. The output voltage of transistor with 560 μm gate width at the beginning and the end of the gate electrode.

electrode. The Fig. 13. shows the distribution of the maximum value of voltage on the drain, gate and source electrodes for a transistor with 560 micro meter gate length when the device is excited by a sinusoidal voltage source (80 GHz).

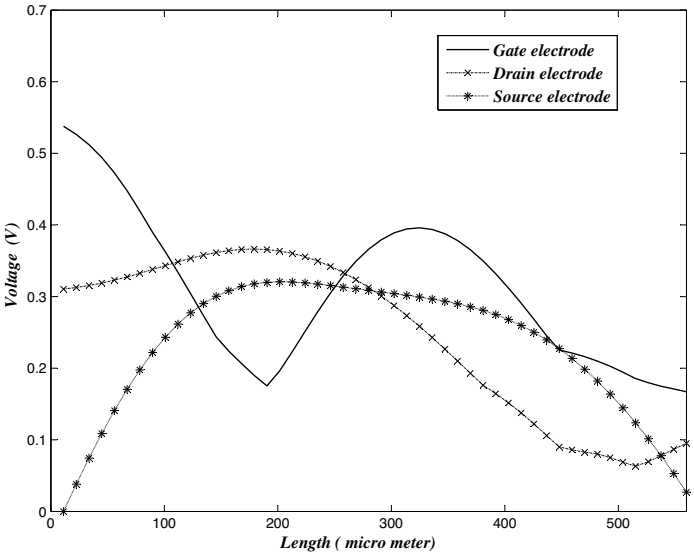

Figure 13. Distribution of the maximum value of the voltage on the drain, gate and source electrodes of a transistor with 560 micro meter gate length.

5. CONCLUSION

A new approach for analysis of microwave/mm-wave transistor has been presented. This new method can consider the effect of wave propagation along the device electrodes, accurately. The derived equation (AMTL) is solved using FDTD technique. The scattering parameters are obtained from the time domain results for 20–220 GHz frequency band. The simulation results show that the proposed method and the slice model have the same results at the low frequency. But, by increasing the frequency to the mm-wave range where the device dimensions are comparable with the wavelength, a difference appears between the results of two models. This is due to the consideration of the wave propagation and the phase cancellation by the proposed model. Moreover, another advantage of this model is the easy of its integration in to CAD optimizers.

ACKNOWLEDGMENT

The authors would like to thank Iran Telecommunication Research Center (ITRC) staffs for supporting this work. They also appreciate Dr. G. Moradi from Amirkabir University of Technology (Tehran Polytechnic) for his good comments.

REFERENCES

1. Goswami, A., M. Gupta, and R. S. Gupta, "Analysis of scattering parameters and thermal noise of a MOSFET for its microwave frequency applications," *Microwave Opt. Technol. Lett.*, Vol. 2, No. 10, 97–105, 2001.
2. Alsunaidi, M. A., S. M. S. Imtiaz, and S. M. Ghazaly, "Electromagnetic wave effects on microwave transistors using a full-wave time-domain model," *IEEE Trans. Microwave Theory Tech.*, Vol. 44, 799–808, 1996.
3. Ghazaly, S. M. and T. Itoh, "Traveling-wave inverted-gate field-effect transistor: concept, analysis, and potential," *IEEE Trans. Microwave Theory Tech.*, Vol. 37, 1027–1032, 1989.
4. Ghazaly, S. M. and T. Itoh, "Inverted-gate field-effect transistors: novel high frequency structures," *IEEE Trans. Electron Devices*, Vol. 35, 810–817, 1988.
5. Goasguen, S., M. Tomeh, and S. M. Ghazaly, "Electromagnetic and semiconductor device simulation using interpolating wavelets," *IEEE Trans. Microwave Theory Tech.*, Vol. 49, No. 12, 2258–2265, 2001.
6. Hussein, Y. A. and S. M. El. Ghazaly, "Modeling and optimization of microwave devices and circuits using genetic algorithms," *IEEE Trans. Microwave Theory Tech.*, Vol. 52, No. 1, 329–336, 2004.
7. Movahhedi, M. and A. Abdipour, "Efficient numerical methods for simulation of high-frequency active device," *IEEE Trans. Microwave Theory Tech.*, Vol. 54, No. 6, 2636–2645, 2006.
8. Movahhedi, M. and A. Abdipour, "Improvement of active microwave device modeling using filter-bank transforms," *Proc. 35th Euro. Microwave., Conf.*, 1113–1117, Paris, France, 2005.
9. Movahhedi, M. and A. Abdipour, "Accelerating the transient simulation of semiconductor devices using filter-bank transforms," *Int. J. Numer. Mod.*, Vol. 19, 47–67, 2006.
10. Abdipour, A. and A. Pacaud, "Complete sliced model of microwave FET's and Comparison with lumped model and

experimental results," *IEEE Trans. Microwave Theory Tech.*, Vol. 44, No. 1, 4–9, 1996.

11. Ongareau, E., R. G. Bosisio, M. Aubourg, J. Obregon, and M. Gayral, "A non-linear and distributed modeling procedure of FETs," *Int. Journal Numerical Modeling*, Vol. 7, 309–319, 1994.
12. Waliullah, M., S. M. Ghazaly, and S. Goodnick, "Large-signal circuit-based time domain analysis of high frequency devices including distributed effects," *Microwave Symposium Digest, IEEE MTT-S International*, Vol. 3, 2145–2148, 2002.
13. Taflove, A., *Computational Electrodynamics the Finite-Difference Time-Domain Method*, Artech House, Norwood, MA, 1996.
14. Paul, C. R., "Incorporation of terminal constraints in the FDTD analysis of transmission lines," *IEEE Trans. Electromagnetic Compatibility*, Vol. 36, 85–91, 1994.
15. Orlandi, A. and C. R. Paul, "FDTD analysis of lossy, multiconductor transmission lines terminated in arbitrary loads," *IEEE Trans. Electromagnetic Compatibility*, Vol. 38, 388–399, 1996.
16. Roden, A. J., C. R. Paul, W. T. Smith, and D. S. Gedney, "Finite-Difference, Time-Domain analysis of lossy transmission lines," *IEEE Trans. Electromagnetic Compatibility*, Vol. 38, 15–24, 1996.
17. Tang, M. and F. J. Mao, "Transient analysis of lossy nonuniform transmission lines using a time-step integration method," *Progress In Electromagnetic Research*, PIER 69, 257–266, 2007.
18. Trakadas, P. T. and C. N. Capsalis, "Validation of a modified FDTD method on non-uniform transmission lines," *Progress In Electromagnetic Research*, PIER 31, 311–329, 2001.
19. Khalaj-Amirhosseini, M., "Analysis of coupled or single nonuniform transmission lines using step-by-step numerical integration," *Progress In Electromagnetic Research*, PIER 58, 187–198, 2006.
20. Khalaj-Amirhosseini, M., "Analysis of periodic and aperiodic coupled nonuniform transmission lines using the Fourier series expansion," *Progress In Electromagnetic Research*, PIER 65, 15–26, 2006.
21. Mondal, J. P., "Distributed scaling approach of MESFETs and its comparison with the lumped-element approach," *IEEE Trans. Microwave Theory Tech.*, Vol. 37, 1085–1090, 1989.
22. Wang, B. Z., X., H. Wang, and J. S. Hong, "On the generalized transmission-line theory," *Journal of Electromagnetic Waves and Applications*, Vol. 19, No. 3, 413–425, 2005.

23. Lin, C. J. and C. C. Chiu, "A novel model extraction algorithm for reconstruction of coupled transmission lines in highspeed digital system," *Journal of Electromagnetic Waves and Applications*, Vol. 19, No. 12, 1595–1609, 2005.
24. Huang, C. C., "Analysis of multiconductor transmission lines with nonlinear terminations in frequency domain," *Journal of Electromagnetic Waves and Applications*, Vol. 19, No. 3, 413–425, 2005.